PHILOSOPHICAL
TRANSACTIONS
— OF —

THE ROYAL
SOCIETY

A

MATHEMATICAL,
PHYSICAL
& ENGINEERING
SCIENCES

Nonlinear optics at maximum coherence

S. E. Harris, G. Y. Yin, M. Jain, H. Xia and A. J. Merriam

Email alerting service	Receive free email alerts when new articles cite this article - sign up in the box at the top right-hand corner of the article or click **here**

Nonlinear optics at maximum coherence

By S. E. Harris, G. Y. Yin, M. Jain, H. Xia and A. J. Merriam

Edward L. Ginzton Laboratory, Stanford University,
Stanford, CA 94305, USA

We describe nonlinear optical processes which use maximum coherence of a non-allowed transition. The nonlinear susceptibility for such processes is of the same order of magnitude as is the linear susceptibility. This allows frequency converters and optical parametric oscillators with bandwidths which are on order of their centre frequency.

1. Introduction

For at least 25 years it has been thought that four-frequency mixing processes are well understood. Figure 1 shows an example of two such processes: (*a*) shows a four-frequency summing process where $\omega_h = (\omega_p - \omega_c) + \omega_l$; (*b*) shows a parametric process which has exponential gain at the signal and idler frequencies ω_s and ω_i.

We begin by considering the excitation of the non-allowed $|1\rangle - |2\rangle$ transition. With a_1 and a_2 as the probability amplitudes of states $|1\rangle$ and $|2\rangle$, and ρ_{12} as the off-diagonal matrix element of the $|1\rangle - |2\rangle$ transition, ρ_{12} is related to the excitation at frequencies ω_p and ω_c by

$$\rho_{12} = a_1 a_2^* \sim (\pm)\Omega_p \Omega_c^* \exp j[(\omega_p - \omega_c)t - (k_p - k_c)z]. \tag{1.1}$$

Noting figure 1, Ω_p, Ω_c, k_p and k_c are the amplitudes of the Rabi frequencies and the k vectors at these frequencies. Table 1 shows how the work of the last five years on electromagnetically induced transparency (EIT) has changed our perspective. In particular, consider the k vector of the excitation $(k_p - k_c)$. In the past, *a priori*, these k vectors were to be evaluated in the nonlinear optical medium. As a result of EIT, to an excellent approximation, even with ω_p and ω_c close to resonance, these k vectors are as in vacuum, i.e. the refractive index at both frequencies is unity. This is of great importance for nonlinear optical processes. Now, we may approach the resonance and use the increased nonlinearity while, at the same time, avoiding the increased (or decreased) refractive index (Harris *et al.* 1990).

The remainder of table 1 shows other consequences of EIT. The relative phase of ρ_{12} (the minus sign) is particularly important. It is because the $|1\rangle - |2\rangle$ transition oscillation is anti-phased with regard to its driving fields that $|a_3|^2 = 0$ and, even when on or near resonance, there is no absorption.

There is also no self-focusing or defocusing as the $|1\rangle - |3\rangle$ transition is approached (Jain *et al.* 1995). Because of this, the $|1\rangle - |2\rangle$ transition may be driven much harder than would otherwise be possible. In particular, we may drive it sufficiently hard that $|\rho_{12}|$ approaches 0.5. This is the condition of maximum coherence.

When at maximum coherence, the nonlinear susceptibility has only a single non-resonant denominator and, therefore, is of the same order of magnitude as the linear
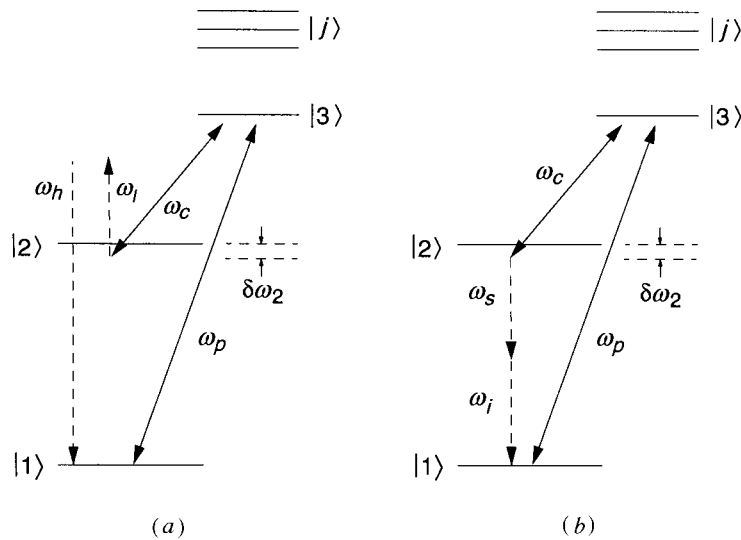
Figure 1. Energy schematic for (*a*) frequency converters and (*b*) optical parametric oscillators which are pumped by population trapped atoms. The pumping frequencies ω_p and ω_c are strong and near resonance. The frequencies ω_l and ω_h for the frequency converter, and ω_s and ω_i for the parametric oscillator are weak. The quantity $\delta\omega_2$ is a small (typically less than 1 GHz) detuning which is used to offset the residual dispersion in the system.

Table 1. *25 years ago and now*

	25 years ago	now
$k_p - k_c$	in medium	as in vacuum
sign	+	−
$|a_3|^2$	finite	0
$|\rho_{12}|$	very small	$\frac{1}{2}$

susceptibility. As a result, the distance in which the interacting frequencies would slip in phase by π radians, i.e. the coherence length, is approximately the same distance in which, in the frequency converter of figure 1*a*, nominally complete photon conversion will occur. It is also the distance in which the parametric gain (figure 1*b*) is approximately $\exp(1)$. This near equality of the nonlinear and linear susceptibilities often leads to frequency converters and amplifiers with bandwidths which are of order of their centre frequencies.

In the following sections of this paper we will first review the key ideas of population trapping and EIT. We then summarize the small signal theory of frequency converters, i.e. $\omega_h = (\omega_p - \omega_c) + \omega_l$, and of optical parametric oscillators, $(\omega_p - \omega_c) = (\omega_s + \omega_i)$. With Pb vapour as an example, we describe experimental results for the frequency converter (Jain *et al.* 1996) and the results of a calculation for the oscillator (Harris & Jain 1997).

2. Population trapped atoms

Because the population of state $|3\rangle$ is zero, the anti-phased atoms described in the previous section are also termed as population trapped (Arimondo 1996). The
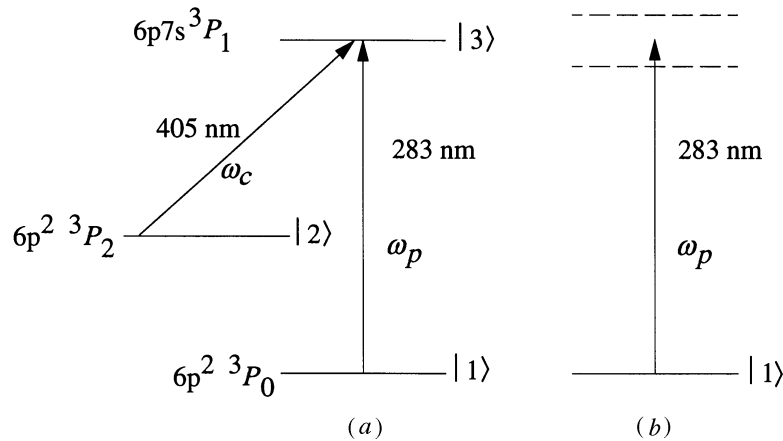
Figure 2. Energy schematic for EIT in Pb vapour. (*a*) Bare state picture. Since it couples states $|2\rangle$ and $|3\rangle$, the 405 nm laser is termed the coupling laser. Since it is sometimes used to probe the absorption which is caused by ground state atoms, the laser at 283 nm, with angular frequency $\omega_{\rm p}$, is called the probe laser. (*b*) Dressed state picture. The frequency of the 283 nm probe beam is equidistant from the dressed states. Because of quantum interference, even when the decay rate of state $|3\rangle$ is large compared to the Rabi frequency of the coupling laser, both the real and imaginary parts of the linear susceptibility are zero.

reader may wonder why we describe the frequency converter or optical parametric oscillator as pumped by these atoms instead of, as is usually done, by the other electromagnetic fields. The reason is that the EIT process which creates the anti-phased atoms involves the time history of the pumping fields at $\omega_{\rm p}$ and $\omega_{\rm c}$.

There are two ways to establish the ensemble of anti-phased driving atoms. The first was demonstrated by Alzetta and co-workers in 1976 (Alzetta *et al.* 1976). In that work, states $|1\rangle$ and $|2\rangle$ were hyperfine ground states of Na which, before the lasers were applied, had roughly equal populations. In this case, the population trapped state results from an optical pumping process and occurs on a time scale of many optical decay times.

The experiments described here require pulsed lasers with pulse lengths which are usually less than 100 ns. Here, as in in experiments of Boller *et al.* (1991) and Field *et al.* (1991), the population trapped state is created by quantum interference. For a single atom, when on resonance, this occurs on a time scale of the inverse Rabi frequency ($1/\Omega_{\rm c}$). With both frequencies detuned from state $|3\rangle$ by $\Delta\omega$, the time scale for establishing EIT by interference is $\Delta\omega/\Omega^2$ (Harris 1994*a*).

3. EIT

Propagation phenomena and, in particular, group velocity delay play an important role in establishing EIT. First consider the case (figure 2) where only a strong field at $\omega_{\rm c}$ is present. This creates the equivalent (dressed) atom shown on the right-hand side of this figure. As shown here, a weak probe beam when tuned to the frequency of the bare $|1\rangle - |2\rangle$ transition is spanned symmetrically by the dressed states. The contributions of these states to the dielectric constant at $\omega_{\rm p}$ interfere so that, in the ideal case of no dephasing on the $|1\rangle - |2\rangle$ transition, the loss and refractive index of the probe beam are zero and unity. But at this same frequency, the medium has a steep, nearly linear, dispersion and a slow group velocity (Harris *et al.* 1992).
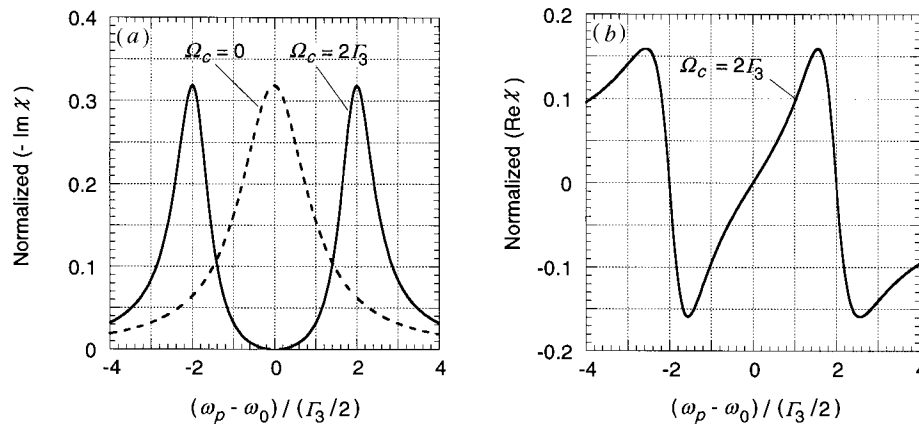
Figure 3. (*a*) Imaginary and (*b*) real parts of the susceptibility of a probe frequency ω_{p} in the presence of a strong-coupling field ω_{c}. The dotted curve of (*a*) is the imaginary part of the susceptibility in the absence of the coupling field. The steep slope versus frequency of the real part of the susceptibility results in the slow group velocity which is characteristic of the preparation phase of EIT. The quantity Γ_3 is the radiative decay rate of state $|3\rangle$. The susceptibilities are normalized so that the integral of the imaginary part is unity.

Figure 3 shows the characteristic shapes of the real and imaginary parts of the linear susceptibility at ω_{p}. It is the slow group velocity which, as described below, leads to a basic energy requirement for EIT.

Perhaps the simplest case to consider occurs when the complex temporal envelopes of the fields at ω_{p} and ω_{c} are the same, but the magnitudes and absolute phases are arbitrary. Such pulses, which are termed as 'matched', are the normal modes of EIT (Harris 1993, 1994*b*). If they are applied to a medium which initially has all of its atoms in the ground state, then one need not do anything special to attain transparency. As the pulses propagate into the medium, the front edge of the probe pulse is delayed with regard to the coupling laser pulse. This allows the quantum interference and transparency to occur. The overall medium becomes transparent in about a group delay time. This delay is proportional to the atom density length product and may be quite long. For example, Kasapi and co-workers have observed a delay of about 60 ns in a 10 cm cell length (Kasapi *et al.* 1995). This corresponds to a group velocity V_{g} such that c/V_{g} is about 160.

It is of importance that the product of the group delay time and the power density of the coupling laser is, to within a small shape factor, nearly constant. For a weak probe beam and a time-invariant coupling laser, the product of the group velocity delay and the photon density of the coupling laser is equal to the oscillator strength weighted number of atoms in the laser path, i.e. if T_{D} is the group delay and P_{c}/A is the power density of the coupling laser at $z = 0$, then

$$T_{\mathrm{D}} = \left(\frac{1}{V_{\mathrm{G}}} - \frac{1}{c}\right) L, \quad \frac{1}{\hbar\omega_{\mathrm{c}}}\left(\frac{P_{\mathrm{c}}}{A}\right) T_{\mathrm{D}} = \frac{f_{13}}{f_{23}} N L. \tag{3.1}$$

This result is, perhaps, the most fundamental requirement for establishing EIT. For pulses which vary slowly compared to their Rabi frequencies, it applies whether on or off resonance and irrespective of the ratio of their Rabi frequencies to each other and to the decay rate Γ_3 from state $|3\rangle$.

The solid and dashed curves in each part of figure 4 show the probe pulse (in local time) at the start and end of a medium (Harris & Luo 1995). Irrespective of the ratio
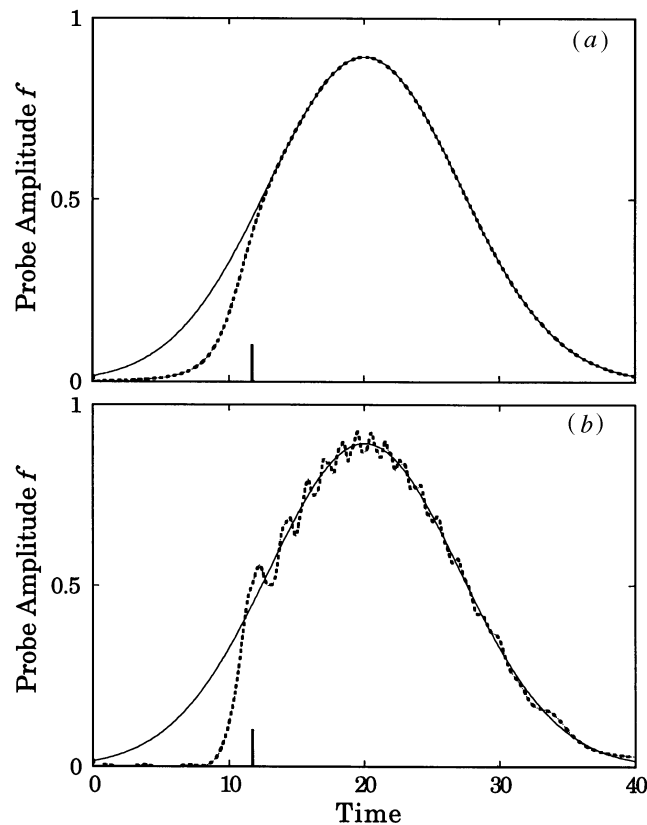
Figure 4. If one applies matched pulses to an optically thick medium, these pulses will self-consistently establish the population-trapped state and, for all time thereafter, will be transmitted without further loss. Both parts of this figure show the pulse at the input (solid line) and at the output (dotted line) of a medium. In both parts, the atom density length product is the same. But the decay rates of state $|3\rangle$ are different; so that in (a), the loss to a probe if alone is $\exp(-5)$ while, in (b), the loss to a probe if alone is $\exp(-5000)$. The output pulse (except for some oscillation) is roughly the same in both cases. Irrespective of the decay rate of state $|3\rangle$, the front edge of the pulse prepares the medium so as to render itself transparent.

of the decay rate Γ_3 to the Rabi frequencies, the pattern is the same. For early times, the medium is opaque and the probe pulse is absorbed. At a critical time, which is roughly the same in both figures, the medium rather abruptly becomes transparent. The upward tick at $\tau = 11.7$ in each figure denotes the time at which the integral of the coupling laser photons from zero to $\tau = 11.7$ is equal to the number of atoms in the path of the laser beam.

When one allows for the $|1\rangle - |2\rangle$ transition linewidth, then there are also constraints on the power density and pulse length of the lasers. (1) When on resonance, the power density of the coupling laser should be sufficiently large that its Rabi frequency exceeds the $|1\rangle - |2\rangle$ transition linewidth. When off resonance, the Rabi frequency is replaced by $\Omega_c^2/\Delta\omega$. (2) The requirements on the pulse length at ω_p depend on its magnitude. For a small probe, there is no requirement and, in fact, the radiation may be incoherent. But if the pulse Rabi frequencies are approximately equal, then the pulse length at ω_p must be short compared to the dephasing time of the $|1\rangle - |2\rangle$ transition.
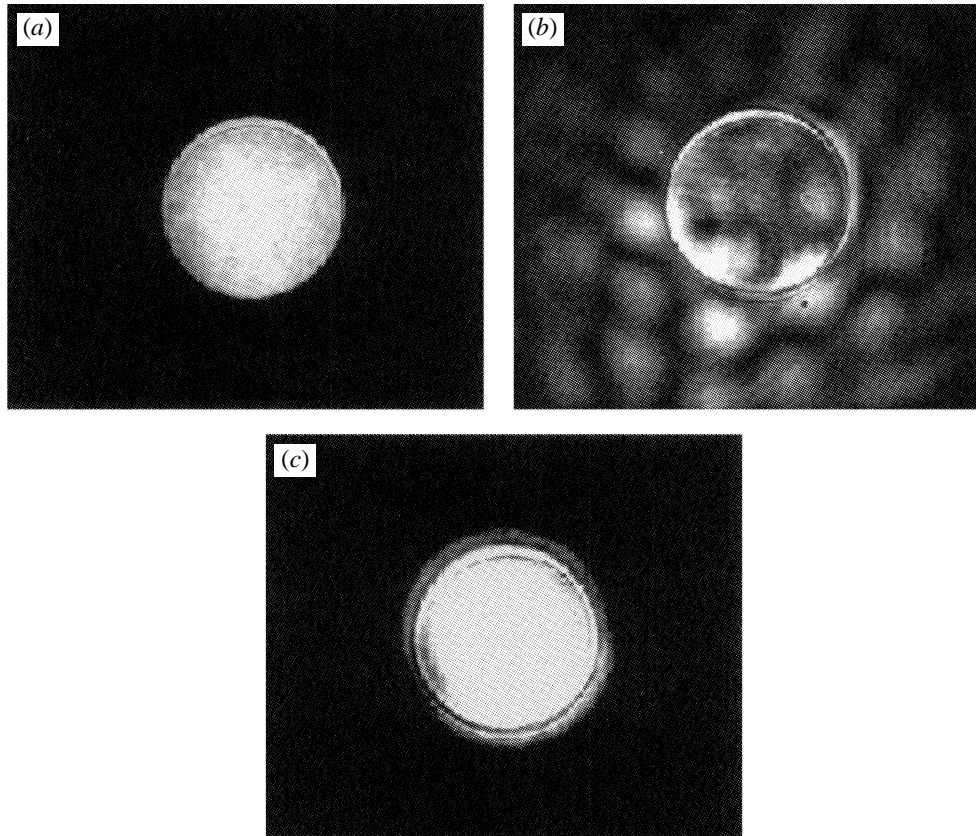
Figure 5. This figure shows how EIT can be used to eliminate optical self-focusing. (*a*) Shows the image of a 3.2 mm aperture as taken with a weak probe beam. (*b*) Shows what happens when the intensity of the probe is increased by about 10 000 times. We see that the laser beam filaments and breaks apart in an uncontrolled manner. In (*c*), the coupling laser is turned on and the image of the aperture is nearly restored.

4. Image transmission

To attain the anti-phased atomic population we will tune both lasers to several cm^{-1} from the $|1\rangle - |3\rangle$ transition. As explained below, this is done to allow control of the phase matching condition. But a probe pulse, if alone, could not propagate near a resonance at high atom densities. As shown in figure 5*b*, such a pulse breaks into an uncontrollable number of filaments. But EIT, just as it eliminates loss on resonance, eliminates near resonance self-focusing and defocusing (figure 5*c*). In the transverse plane of a propagating beam or image, both the amplitude and phase of the E fields at ω_{p} and ω_{c} vary as a function of radius. But, as part of the preparation process, the phase and amplitudes of the density matrix elements ρ_{12} self-adjust so as to allow transmission (Jain *et al.* 1995).

5. Earlier work

Before proceeding further, we note earlier work showing the connection between EIT and nonlinear optics. Harris *et al.* (1990) noted how EIT allows a destructive interference in the linear susceptibility while, at the same time, allowing a construc-

tive interference in the nonlinear susceptibility. This is not obvious: for example, earlier, Tewari & Agarwal (1986) had shown how a strong field, which is not in the loop of generating and generated frequencies, may be used to control phase matching in a dense medium. But, in such a system, though still useful, the linear and nonlinear susceptibilities both interfere destructively and have a zero at the same frequency.

The constructive versus destructive interference was first demonstrated by Hakuta and Stoicheff (Hakuta *et al.* 1991, 1992) in atomic hydrogen and their continuing experiments show the utility of EIT for the generation of VUV radiation.

In other early and continuing work, Hemmer *et al.* (1995) have shown the use of EIT for optical phase conjugation at very low power. Jain *et al.* (1993) have shown the increase in efficiency which occurs as Ω_c exceeds the $|1\rangle - |2\rangle$ transition linewidth. Rathe *et al.* (1993) have described nonlinear index effects involving EIT. Recently, Schmidt & Imamoglu (1996) have described a new method for EIT enhanced cross-phase modulation.

There are also overlaps with the now substantial literature on the propagation dynamics of EIT (Grobe *et al.* 1994; Fleischhauer & Manka 1996; Cerboneschi & Arimondo 1995), as well as on lasers without population inversion (Kocharovskaya & Mandel 1994; Padmabandu *et al.* 1996), and on near-resonance enhancement of the refractive index (Scully 1991).

6. Theory

The pumping atoms are characterized by the density matrix elements ρ_{ij} of the $|1\rangle - |2\rangle$ transition. Because the fields at ω_p and ω_c are strong and near resonance, and the other fields are weak and also, typically, far from resonance, the ρ_{ij} are determined by ω_p and ω_c. When at maximum coherence, the magnitude of each of the density matrix elements is 0.5. The phase of ρ_{12}, as a function of distance, may be controlled by a small detuning from the two-photon (Raman) resonance, and an expression for this phase variation is given later. In this section, the ρ_{ij} are to be treated as known functions of z.

We assume that all of the fields are monochromatic with slowly varying spatial envelopes. We also assume that the detuning of these fields from the virtual states which determine the effective susceptibilities are large compared to the linewidths of these states. These states may then be eliminated and the behaviour of the system is then characterized by the constants

$$\left.\begin{aligned}
a_q &= \frac{1}{2\hbar^2} \sum_j \left[\frac{|\mu_{1j}|^2}{(\omega_j - \omega_1) - \omega_q} + \frac{|\mu_{1j}|^2}{(\omega_j - \omega_1) + \omega_q} \right], \\
d_q &= \frac{1}{2\hbar^2} \sum_j \left[\frac{|\mu_{2j}|^2}{(\omega_j - \omega_2) - \omega_q} + \frac{|\mu_{2j}|^2}{(\omega_j - \omega_2) + \omega_q} \right], \\
b_q &= \frac{1}{2\hbar^2} \sum_j \left[\frac{\mu_{1j}\mu_{2j}}{(\omega_j - \omega_1) - \omega_q} + \frac{\mu_{1j}\mu_{2j}}{(\omega_j - \omega_2) + \omega_q} \right], \\
c_q &= b_q^*.
\end{aligned}\right\} \tag{6.1}$$

Here, ω_j are the energies of the (virtual) states $|j\rangle$ and μ_{ij} are the matrix elements from states $|1\rangle$ and $|2\rangle$ to state $|j\rangle$ (see figure 1).

(*a*) *Frequency converter*

In the frequency converter (Jain *et al.* 1996), we apply a frequency ω_l to generate a frequency ω_h (figure 1*b*)

$$\omega_{\mathrm{h}} = (\omega_2 - \omega_1) + \omega_{\mathrm{l}}. \tag{6.2}$$

The equations for the envelopes of the fields as a function of distance are

$$\left.\begin{aligned}
\frac{\partial E_{\mathrm{h}}}{\partial z} &= -j\eta_{\mathrm{h}}\hbar\omega_{\mathrm{h}}N[(a_{\mathrm{h}}\rho_{11} + d_{\mathrm{h}}\rho_{22})E_{\mathrm{h}} + b_{\mathrm{h}}\rho_{12}E_{\mathrm{l}}], \\
\frac{\partial E_{\mathrm{l}}}{\partial z} &= -j\eta_{\mathrm{l}}\hbar\omega_{\mathrm{l}}N[(a_{\mathrm{l}}\rho_{11} + d_{\mathrm{l}}\rho_{22})E_{\mathrm{l}} + c_{\mathrm{h}}\rho_{12}^{*}E_{\mathrm{h}}].
\end{aligned}\right\} \tag{6.3}$$

The quantity N is the atom density, $\eta = (\mu/\epsilon_0)^{1/2}$, and ρ_{ij} are the density matrix elements of the $|1\rangle - |2\rangle$ transition. The k vectors, k_{l} and k_{h}, *relative to vacuum*, and the coupling constants κ_{h} and κ_{l} are

$$\left.\begin{aligned}
k_{\mathrm{h}} &= \eta_{\mathrm{h}}\hbar\omega_{\mathrm{h}}N(a_{\mathrm{h}}\rho_{11} + d_{\mathrm{h}}\rho_{22}), \quad k_{\mathrm{l}} = \eta_{\mathrm{l}}\hbar\omega_{\mathrm{l}}N(a_{\mathrm{l}}\rho_{11} + d_{\mathrm{l}}\rho_{22}), \\
\kappa_{\mathrm{h}} &= \eta_{\mathrm{h}}\hbar\omega_{\mathrm{h}}Nb_{\mathrm{h}}|\rho_{12}|, \quad \kappa_{\mathrm{l}} = \eta_{\mathrm{l}}\hbar\omega_{\mathrm{l}}Nc_{\mathrm{h}}|\rho_{12}|.
\end{aligned}\right\} \tag{6.4}$$

We write the coherence ρ_{12} and the k vector mismatch Δk as

$$\rho_{12} = |\rho_{12}|\exp{-j\delta kz}, \quad \Delta k = \delta k - (k_{\mathrm{h}} - k_{\mathrm{l}}) \tag{6.5}$$

and change variable by $\tilde{E}_{\mathrm{h}} = E_{\mathrm{h}}\exp(jk_{\mathrm{h}}z)$ and $\tilde{E}_{\mathrm{l}} = E_{\mathrm{l}}\exp(jk_{\mathrm{l}}z)$. With the boundary condition $\tilde{E}_{\mathrm{h}}(0) = 0$, the solution of equation (6.3) is

$$\left.\begin{aligned}
\tilde{E}_{\mathrm{l}}(z) &= \tilde{E}_{\mathrm{l}}(0)(\exp j\tfrac{1}{2}\Delta kz)\left(\cos sz - j\frac{\Delta k}{2s}\sin sz\right), \\
\tilde{E}_{\mathrm{h}}(z) &= -j\frac{\kappa_{\mathrm{h}}}{s}\tilde{E}_{\mathrm{l}}(0)(\exp -j\tfrac{1}{2}\Delta kz)\sin sz,
\end{aligned}\right\} \tag{6.6}$$

where

$$s = (\kappa_{\mathrm{l}}\kappa_{\mathrm{h}} + \tfrac{1}{4}\Delta k^2)^{1/2}.$$

The frequency converter solution conserves photons between ω_{l} and ω_{h}. With $\Delta k = 0$, a photon conversion efficiency of unity is obtained at a distance z such that $\sqrt{\kappa_{\mathrm{l}}\kappa_h}z = \tfrac{1}{2}\pi$.

(*b*) *Parametric oscillator*

In the parametric oscillator (Harris & Jain 1997), the signal and idler fields are related by (figure 1*b*)

$$\omega_{\mathrm{i}} = (\omega_2 - \omega_1) - \omega_{\mathrm{s}} \tag{6.7}$$

and, if either grows with distance, the other must grow. There is parametric gain and the process may start from either classical or quantum noise.

The coupled equations for the E fields at ω_{s} and ω_{i} are

$$\left.\begin{aligned}
\frac{\partial E_{\mathrm{s}}}{\partial z} &= -j\eta_{\mathrm{s}}\hbar\omega_{\mathrm{s}}N[(a_{\mathrm{s}}\rho_{11} + d_{\mathrm{s}}\rho_{22})E_{\mathrm{s}} + b_{\mathrm{s}}\rho_{12}E_{\mathrm{i}}^{*}], \\
\frac{\partial E_{\mathrm{i}}}{\partial z} &= -j\eta_{\mathrm{i}}\hbar\omega_{\mathrm{i}}N[(a_{\mathrm{i}}\rho_{11} + d_{\mathrm{i}}\rho_{22})E_{\mathrm{i}} + c_{\mathrm{s}}\rho_{12}E_{\mathrm{s}}^{*}].
\end{aligned}\right\} \tag{6.8}$$

Here, the k vectors (relative to vacuum) and coupling constants are

$$\left.\begin{array}{ll} k_\mathrm{s} = \eta_\mathrm{s}\hbar\omega_\mathrm{s}N(a_\mathrm{s}\rho_{11} + d_\mathrm{s}\rho_{22}), & k_\mathrm{i} = \eta_\mathrm{i}\hbar\omega_\mathrm{i}N(a_\mathrm{i}\rho_{11} + d_\mathrm{i}\rho_{22}), \\ \kappa_\mathrm{s} = \eta_\mathrm{s}\hbar\omega_\mathrm{s}Nb_\mathrm{s}|\rho_{12}|, & \kappa_\mathrm{i} = \eta_\mathrm{i}\hbar\omega_\mathrm{i}Nb_\mathrm{s}^*|\rho_{12}| \end{array}\right\} \tag{6.9}$$

and ρ_{12} and Δk are defined as

$$\rho_{12} = |\rho_{12}|\exp{-j\delta kz}, \quad \Delta k = \delta k - (k_\mathrm{s} + k_\mathrm{i}). \tag{6.10}$$

With the change of variable $\tilde{E}_\mathrm{s} = E_\mathrm{s}\exp(jk_\mathrm{s}z)$ and $\tilde{E}_\mathrm{i} = E_\mathrm{i}\exp(jk_\mathrm{i}z)$, and the boundary condition $\tilde{E}_\mathrm{i}(0) = 0$, the solution of equation (6.8) is

$$\left.\begin{array}{l} \tilde{E}_\mathrm{s}(z) = \tilde{E}_\mathrm{s}(0)(\exp{-j\tfrac{1}{2}\Delta kz})\left(\cosh sz + j\dfrac{\Delta k}{2s}\sinh sz\right), \\[3mm] \tilde{E}_\mathrm{i}^*(z) = j\dfrac{\kappa_\mathrm{i}}{s}\tilde{E}_\mathrm{s}(0)(\exp{j\tfrac{1}{2}\Delta kz})\sinh sz, \end{array}\right\} \tag{6.11}$$

where

$$s = (\kappa_\mathrm{s}\kappa_\mathrm{i} - \tfrac{1}{4}\Delta k^2)^{1/2}.$$

If ρ_{12} contains no spatial dependence over and above vacuum, i.e. $\delta k = 0$, then, using the constants of equation (6.1), we find that the parameter s is imaginary and, therefore, there is no parametric gain. Gain is obtained by adjusting the two-photon detuning $\delta\omega_2$ of the pump and coupling lasers (figure 1) so as to set $\Delta k = 0$ at band centre.

7. Phase matching

One may show that, for two-photon detunings $\delta\omega_2$, which are small compared to $d_\mathrm{c}|E_\mathrm{c}|^2$, $|\rho_{11}| = |\rho_{22}| = -\rho_{12} = 0.5$, and the spatially varying phase δkz of ρ_{12} is

$$\delta k = -\tfrac{1}{2}(k_\mathrm{p}^{(0)} + k_\mathrm{c}^{(0)})\frac{\delta\omega_2}{d_\mathrm{c}|E_\mathrm{c}|^2}. \tag{7.1}$$

Here, the quantities $k_\mathrm{p}^{(0)} = \eta_\mathrm{p}\hbar\omega_\mathrm{p}Na_\mathrm{p}$ and $k_\mathrm{c}^{(0)} = \eta_\mathrm{c}\hbar\omega_\mathrm{c}Nd_\mathrm{c}$ are the k vectors (relative to vacuum) of the fields at frequencies ω_p and ω_c if all of the atoms are in state $|1\rangle$ or state $|2\rangle$, respectively. Because these quantities are very large as compared to the non-resonant a_q and d_q evaluated at the signal and idler frequencies, only small detunings (typically under a GHz) of $\delta\omega_2$ are necessary to attain phase matching.

8. Pb vapour frequency converter

We have recently reported experimental results for a near-maximum coherence frequency up-conversion experiment in Pb vapour (Jain *et al.* 1996). The experimental setup for this work was similar to that of Jain *et al.* (1995) and Kasapi *et al.* (1995). As shown in figure 2*a*, the coherence is established by a 406 nm coupling laser and a 283 nm probe laser. The laser to be up-converted, ω_l, has a wavelength of 425 nm. These wavelengths are obtained by frequency doubling or frequency tripling the output of a single longitudinal mode, injection seeded, Ti : sapphire laser system. The pulse durations of the probe, coupling and 425 nm laser pulses are 22, 39 and 26 ns, respectively. The generated wavelength is at 293 nm and has a pulse length of 21 ns. The detuning of the 293 nm beam from state $|3\rangle$ (figure 1) is 1112 cm^{-1}.
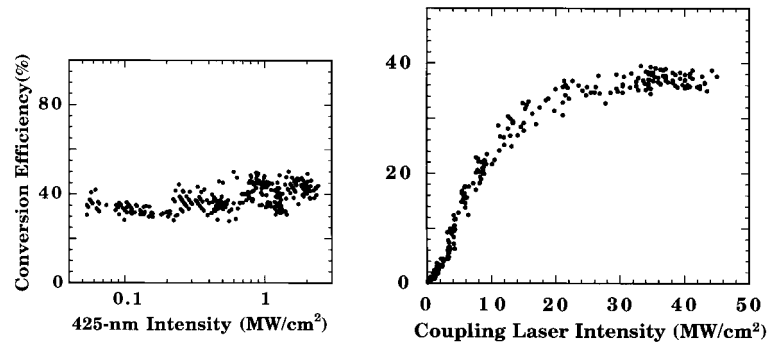
Figure 6. (Left) Conversion efficiency versus 425 nm intensity. The conversion efficiency is constant at *ca.* 40%. For this data, $N = 4.9 \times 10^{15} \pm 20\%$ atoms cm^{-3}, $\gamma_{21}^{-1} = 28$ ns, and the probe and coupling laser intensities are 12 and 30 MW cm^{-2}, respectively.

Figure 7. (Right) Conversion efficiency versus coupling laser intensity. For this data, $N = 3.7 \times 10^{15} \pm 20\%$ atoms cm^{-3}, $\gamma_{21}^{-1} \sim 20$ ns, and the probe and 425 nm intensities are 11 and 1.9 MW cm^{-2}, respectively.

The experiment was done with 99.97% isotopically pure lead vapour (^{208}Pb). This expensive isotope was used in order to avoid hyperfine structure. The probe and coupling lasers had opposite circular polarizations, thereby creating an ideal three state system. The fused-silica sidearm cell was 25.4 cm and was operated at a typical atom density of 5×10^{15} atoms cm^{-3}. This density was measured as in Kasapi *et al.* (1996). At our operating atomic density × length product, a resonant, weak-probe laser alone would see an absorption-length product of $\alpha L = 3 \times 10^5$ and a transmission of $\exp(-\alpha L)$. At this operating density, the dephasing time of the $|1\rangle - |2\rangle$ transition was about 28 ns and, because of out-gassing of the silica cell, varied by about a factor of two.

The data for this experiment was collected by fast photodetectors connected to a 5 Gsample/s Textronix TDS 684A four-channel, real-time, digitizing oscilloscope. The data shown in figures 6 and 7 are from individual pulses with no averaging, while the data for figure 8 are averaged over 30 shots.

We define the term 'conversion efficiency' as the ratio of the generated power density at 293 nm to the input power density at 425 nm *in the spatially and temporally overlapped portions of the beams.* The conversion efficiency if the power densities of all of the laser beams are included is about 0.5%.

Figure 6 shows the conversion efficiency from 425 to 293 nm as a function of the 425 nm intensity. The intensities of the probe and coupling lasers for this data are 12 and 30 MW cm^{-2}, respectively. As expected from equation (6.6), the conversion efficiency is constant at *ca.* 40%, as the 425 nm intensity is varied over about two orders of magnitude.

In figure 7, we show the conversion efficiency as a function of the coupling laser intensity. For these data, the intensities of the probe and 425 nm lasers are 11 and 1.9 MW cm^{-2}, respectively, and the cell density is $N = 3.7 \times 10^{15}$ atoms cm^{-3}. As the coupling laser intensity is increased, the conversion efficiency first improves linearly and then reaches a maximum value of about 39%. In the linear region, the energy density of the coupling laser is not sufficient to satisfy the atom preparation condition of equation (3.1).

In figure 8, we show the conversion efficiency as a function of small detunings from the two-photon resonance. The two-photon detuning is precisely controlled by very
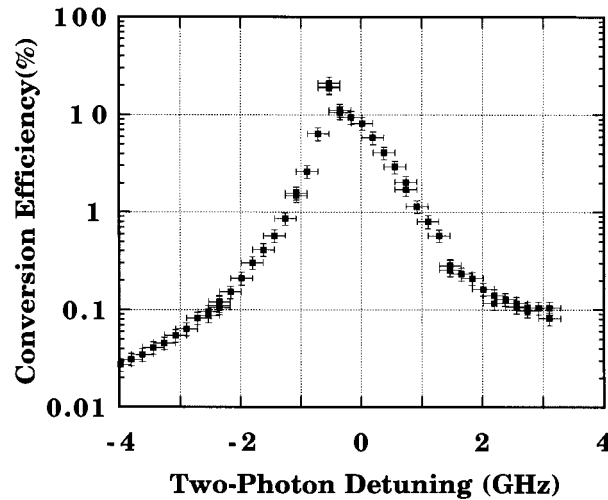
Figure 8. Conversion efficiency versus two-photon detuning. For this data, $N = 4.9 \times 10^{15} \pm 20\%$ atoms cm^{-3}, $\gamma_{21}^{-1} = 14$ ns, $I_p = 13$, $I_c = 22$ and $I_e = 2.8$ MW cm^{-2}. The maximum conversion efficiency is *ca.* 20%.

small changes in the frequency of the probe laser. At exact two-photon resonance (determined by maximizing the EIT effect for a weak probe beam), the conversion efficiency is about 10%. At a two-photon detuning of *ca.* -0.5 GHz, we achieve a conversion efficiency of *ca.* 20%. As noted in equation (7.1), small detunings from two-photon resonance affect the phase of the probe and coupling lasers, thereby allowing compensation for a small phase mismatch.

9. Parametric gain and spontaneous emission

Figure 1*b* is an energy level schematic for an optical parametric oscillator which is pumped by population trapped atoms. The degenerate frequency is $\omega_s = \omega_i = \frac{1}{2}(\omega_2 - \omega_1)$. In Pb vapour, the pumping fields at ω_p and ω_c are the same as for the frequency converter of the previous section; but here, at a sufficient atom density $\times$ length product and for sufficient pumping intensity, there is parametric gain over much of the infrared and far-infrared spectrum.

To illustrate the possibilities for this type of device we assume a cell length of 25 cm and an atom density of 5×10^{16} atoms cm^{-3}. (This density is about ten times larger than we are now able to obtain using the fused quartz sidearm cell, but could be obtained by using a heat pipe.) We choose power densities at ω_p and ω_c so as to equalize the Rabi frequencies of these fields. Taking the power density at ω_p as 100 MW cm^{-2}, and that at ω_c as 32.7 MW cm^{-2}, the Rabi frequencies are $\Omega_p = \Omega_c = 9.17$ cm^{-1}.

Figure 9 shows the parametric (power) gain as a function of frequency. Here, $\delta\omega_2$ is chosen so as to set $\Delta k = 0$ at line centre and is not varied as the signal frequency varies. The gain peaks at the degenerate frequency of $\frac{1}{2}(\omega_2 - \omega_1) = 5325$ cm^{-1}, and remains within 50% of its maximum over a bandwidth of 7560 cm^{-1}. To attain phase matching at line centre requires a two-photon detuning of -110 MHz. (For detunings which are within the rotating wave approximation, this value is independent of the common detuning of the pump and coupling laser from state $|3\rangle$.)

It should be noted that the gain of figure 9 may, instead, be interpreted (see equa-
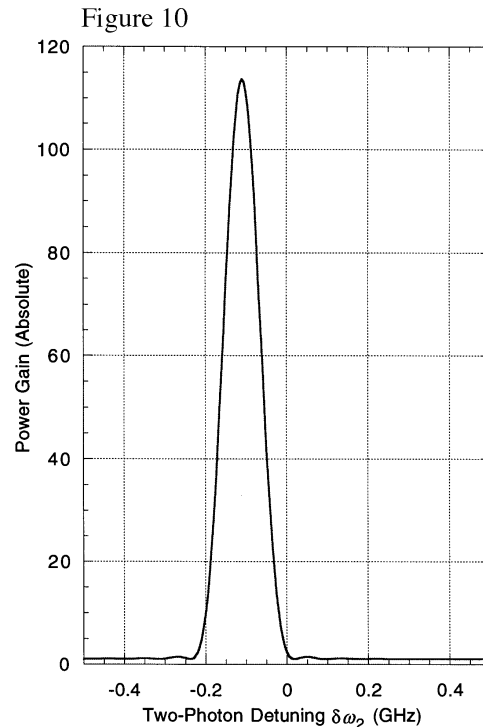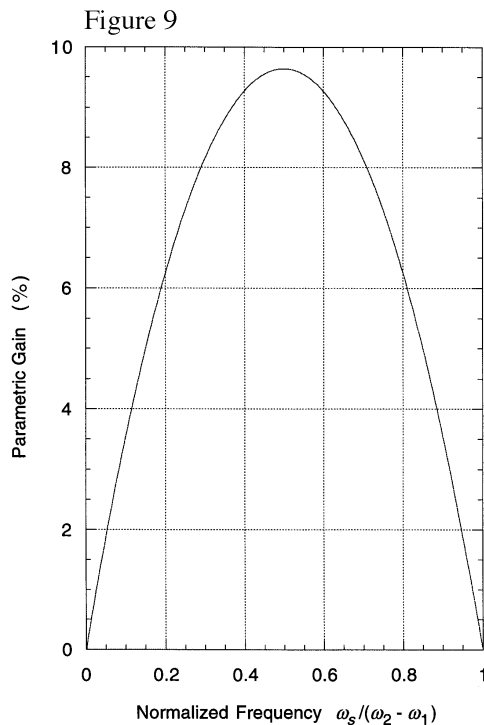
Figure 9

Figure 10

Figure 9. Parametric gain versus normalized signal frequency. For Pb vapour, the gain maximizes at $1.88\,\mu\text{m}$ and has a bandwidth of about $7500\,\text{cm}^{-1}$.

Figure 10. Power gain versus two-photon detuning. For this figure, the atom density is $N = 5 \times 10^{16}$ atoms cm^{-3} and the cell length is $L = 2.5\,\text{m}$.

tion (6.11)) as the photon conversion efficiency from the signal to the idler. Therefore, if one used a conventional optical parametric oscillator to generate radiation in the 0.94–$1.88\,\mu\text{m}$ spectral region, the Pb cell, acting as a frequency down-converter, and with fixed $\delta\omega_2$, would generate radiation which is tunable from $1.88\,\mu$ to nearly d.c.

Figure 10 shows the importance of the ability to adjust the quantity δk of equation (6.10). If $\delta\omega_2 = \delta k = 0$, there is no parametric gain. A small (*ca.* $0.11\,\text{GHz}$) and fixed detuning of either the pump or coupling laser is sufficient to establish the broadband gain of figure 9.

We also note that even when the loss in the path of the signal and idler frequencies exceeds the gain, the parametric spontaneous emission at these frequencies will still be present and will vary as the square of the number density $\times$ length product, and linearly with the amplifier bandwidth (Harris *et al.* 1967; Byer & Harris 1968). This emission will peak in the forward direction, and does not require a population inversion between states $|1\rangle$ and $|2\rangle$.

10. Summary

We have described frequency conversion and optical parametric gain processes which are pumped by an anti-phased ensemble of population trapped atoms. The atoms are driven, using electromagnetically induced transparency, by near-resonance lasers. The relative phase of the atoms, as a function of distance, is controlled by a

small detuning from two-photon resonance. When the $|\rho_{12}| = \frac{1}{2}$, the nonlinear and linear susceptibilities both have a single non-resonant denominator and are of the same order of magnitude. This results in frequency converters, parametric amplifiers and sources of spontaneous photons which have bandwidths which may be of the order of their centre frequencies.

References

Alzetta, G., Gozzini, A., Moi, L. & Orriols, G. 1976 An experimental method for the observation of rf transitions and laser beat resonances in oriented Na vapour. *Nuovo Cimento* B **36**, 5–20.

Arimondo, E. 1996 Coherent population trapping in laser spectroscopy. In *Progress in optics* (ed. E. Wolf), pp. 257–354. New York: Elsevier.

Boller, K.-J., Imamoglu, A. & Harris, S. E. 1991 Observation of electromagnetically induced transparency. *Phys. Rev. Lett.* **66**, 2593–2596.

Byer, R. L. & Harris, S. E. 1968 Power and bandwidth of spontaneous parametric emission. *Phys. Rev.* **168**, 1064–1068.

Cerboneschi, E. & Arimondo, E. 1995 Transparency and dressing for optical pulse pairs through a double-λ absorbing medium. *Phys. Rev.* A **52**, R1823–R1826.

Field, J. E., Hahn, K. H. & Harris, S. E. 1991 Observation of electromagnetically induced transparency in collisionally broadened lead vapour. *Phys. Rev. Lett.* **67**, 3062–3065.

Fleischhauer, M. & Manka, A. S. 1996 Propagation of laser pulses and coherent population transfer in dissipative three-level systems: an adiabatic dressed-state picture. *Phys. Rev.* A **54**, 794–803.

Grobe, R., Hioe, F. T. & Eberly, J. H. 1994 Formation of shape-preserving pulses in a nonlinear adiabatically integrable system. *Phys. Rev. Lett.* **73**, 3183–3186.

Hakuta, K., Marmet, L. & Stoicheff, B. P. 1991 Electric-field-induced second-harmonic generation with reduced absorption in atomic hydrogen. *Phys. Rev. Lett.* **66**, 596–599.

Hakuta, K., Marmet, L. & Stoicheff, B. P. 1992 Nonlinear optical generation with reduced absorption using electric-field coupling in atomic hydrogen. *Phys. Rev.* A **45**, 5152–5159.

Harris, S. E. 1993 Electromagnetically induced transparency with matched pulses. *Phys. Rev. Lett.* **70**, 552–555.

Harris, S. E. 1994a Refractive index control with strong fields. *Opt. Lett.* **19**, 2018–2020.

Harris, S. E. 1994b Normal modes for electromagnetically induced transparency. *Phys. Rev. Lett.* **72**, 52–55.

Harris, S. E. & Jain, M. 1997 Optical parametric oscillators pumped by population trapped atoms. *Opt. Lett.* **22**, 636–638.

Harris, S. E. & Luo, Z.-F. 1995 Preparation energy for electromagnetically induced transparency. *Phys. Rev.* A **52**, R928–R931.

Harris, S. E., Oshman, M. K. & Byer, R. L. 1967 Observation of tunable optical parametric fluorescence. *Phys. Rev. Lett.* **18**, 732–734.

Harris, S. E., Field, J. E. & Imamoglu, A. 1990 Nonlinear optical processes using electromagnetically induced transparency. *Phys. Rev. Lett.* **64**, 1107–1110.

Harris, S. E., Field, J. E. & Kasapi, A. 1992 Dispersive properties of electromagnetically induced transparency. *Phys. Rev.* A **46**, R29–R32.

Hemmer, P. R., Katz, D. P., Donoghue, J., Cronin-Golomb, M., Shahriar, M. S. & Kumar, P. 1995 Efficient low-intensity optical phase conjugation based on coherence population trapping in sodium. *Opt. Lett.* **20**, 982–984.

Jain, M., Yin, G. Y., Field, J. E. & Harris, S. E. 1993 Observation of electromagnetically induced phasematching. *Opt. Lett.* **18**, 998–1000.

Jain, M., Merriam, A. J., Kasapi, A., Yin, G. Y. & Harris, S. E. 1995 Elimination of optical self-focusing by population trapping. *Phys. Rev. Lett.* **75**, 4385–4388.

Jain, M., Xia, H., Yin, G. Y., Merriam, A. J. & Harris, S. E. 1996 Efficient nonlinear frequency conversion with maximal atomic coherence. *Phys. Rev. Lett.* **77**, 4326–4329.

Kasapi, A., Jain, M., Yin, G. Y. & Harris, S. E. 1995 Electromagnetically induced transparency: propagation dynamics. *Phys. Rev. Lett.* **74**, 2447–2450.

Kasapi, A., Yin, G. Y., Jain, M. & Harris, S. E. 1996 Measurement of Lorentzian linewidths by pulse propagation delay. *Phys. Rev. A* **53**, 4547–4555.

Kocharovskaya, O. & Mandel, P. 1994 Basic models of lasing without inversion: general form of amplification condition and problem of self-consistency. *Quantum Opt.* **6**, 217–230.

Padmabandu, G. G., Welch, G. R., Shubin, I. N., Fry, N. S., Nikonov, D. E., Lukin, M. D. & Scully, M. O. 1996 Laser oscillation without population inversion in a sodium atomic beam. *Phys. Rev. Lett.* **76**, 2053–2056.

Rathe, U., Fleischhauer, M., Zhu, S. Y., Hänsch, T. W. & Scully, M. O. 1993 Nonlinear theory of index enhancement via quantum coherence and interference. *Phys. Rev. A* **47**, 4994–5002.

Schmidt, H. & Imamoglu, A. 1996 Giant Kerr nonlinearities obtained by electromagnetically induced transparency. *Opt. Lett.* **21**, 1936–1938.

Scully, M. O. 1991 Enhancement of the index of refraction via quantum coherence. *Phys. Rev. Lett.* **67**, 1855–1858.

Tewari, S. P. & Agarwal, G. S. 1986 Control of phase matching and nonlinear generation in dense media by resonant fields. *Phys. Rev. Lett.* **56**, 1811–1814.